

Hydrogen and Copper Ion-Induced Molecular Reorganizations in Scorpionand-like Ligands. A Potentiometric, Mechanistic, and Solid-State Study

Begoña Verdejo,[†] Armando Ferrer,[‡] Salvador Blasco,[†] Carmen Esther Castillo,[‡] Jorge González,[†] Julio Latorre,[§] M. Angeles Máñez,[‡] Manuel García Basallote,^{*,‡} Conxa Soriano,^{||} and Enrique García-España^{*,†}

Departamento de Química Inorgánica, Instituto de Ciencia Molecular, Universidad de Valencia, Edificio de Institutos de Paterna, Apdo 22085, 46071 Valencia, Spain, Departamento de Ciencia de los Materiales e Ingeniería Metalúrgica, Facultad de Ciencias, Universidad de Cádiz, Apdo 40, Puerto Real, 11510 Cádiz, Spain, Departamento de Química Inorgánica, Instituto de Materiales de la Universidad de Valencia, Universidad de Valencia, C/ Dr. Moliner 50, 46100 Burjassot (Valencia), Spain, and Departamento de Química Orgánica, Instituto de Ciencia Molecular, Universidad de Valencia, Edificio de Institutos de Paterna, Apdo 22085, 46071 Valencia, Spain

Received April 4, 2007

Two aza scorpionand-like macrocycles (**L2** and **L3**) have been prepared. **L2** consists of a tren amine with two of its arms cyclized with a 2,6-bis(bromomethyl)pyridine. In **L3**, the remaining pendant arm has been further functionalized with a fluorophoric naphthalene group. X-ray data on the compounds $[\text{H}(\mathbf{L3})]\text{ClO}_4 \cdot \text{H}_2\text{O}$ (**1**) and $[\text{H}_3(\mathbf{L3})](\text{H}_2\text{PO}_4)_3 \cdot \text{H}_2\text{O}$ (**2**) as well as solution studies (pH-metry, UV–vis, and fluorescence data) show the movement of the pendant arm as a result of the protonation degree of the macrocycles and of the formation of intramolecular hydrogen bonds. X-ray data on the complexes $[\text{Cu}(\mathbf{L2})](\text{ClO}_4)_2 \cdot \text{H}_2\text{O}$ (**3**) and $[\text{Cu}(\mathbf{L3})](\text{ClO}_4)_2$ (**4**) and solution studies on Cu^{2+} coordination show the implication of the nitrogen of the arm in the binding to the metal ion. Kinetic studies on the decomposition and formation of the Cu^{2+} complexes provide additional information about the pH-dependent molecular reorganizations. Moreover, the obtained information suggests that the kinetics of the tail on/off process is essentially independent of the lability of the metal center.

Introduction

Controlled molecular movements and reorganizations constitute a research topic of great interest.^{1–6} This interest stems from the key role that molecular machines and molecular reorganizations have in living systems. ATP hydrolysis and proton-motive forces power these move-

ments. Examples of movements coupled to proton gradients are, for instance, the rotation of the γ protein that acts as an axle of the $\alpha_3\beta_3$ hexamer in the F_0/F_1 ATP-synthase⁷ and the molecular gear generating the propulsive force that induces flagellar rotation in bacteria.⁸ The regulatory role of many proteins like calmoduline is also related to conformational changes induced by protonation processes.⁹ Molecular chaperonins that take care of the correct folding of proteins¹⁰ and the puncturing device of bacteriophages¹¹ are very interesting molecular machines driven by ATP hydroly-

* To whom correspondence should be addressed. E-mail: enrique.garcia-es@uv.es (E.G.-E.), manuel.basallote@uca.es (M.G.B.).

[†] Instituto de Ciencia Molecular, Universidad de Valencia.

[‡] Universidad de Cádiz.

[§] Instituto de Materiales, Universidad de Valencia.

^{||} Instituto de Ciencia Molecular, Universidad de Valencia.

- (1) Raehm, L.; Sauvage, J.-P. *Struct. Bonding (Berlin)* **2001**, *99*, 55.
- (2) Rease, A. P.; Jeppesen, J. O.; Stoddart, J. F.; Luio, Y.; Collier, C. P.; Heath, J. R. *Acc. Chem. Res.* **2001**, *34*, 433.
- (3) Ballardini, R.; Balzani, V.; Credi, A.; Gaudolfi, M. T.; Venturi, M. T. *Acc. Chem. Res.* **2001**, *34*, 445.
- (4) Amendola, V.; Fabbrizzi, L.; Mangano, C.; Pallavicini, P. *Acc. Chem. Res.* **2001**, *34*, 488.
- (5) Feringa, B. L. *Acc. Chem. Res.* **2001**, *34*, 504.
- (6) Kinbara, K.; Aida, T. *Chem. Rev.* **2005**, *105*, 1377.

- (7) (a) Yoshida, M.; Muneyuki, M.; Hisabori, T. *Nat. Rev. Mol. Cell Biol.* **2001**, *2*, 669. (b) Boyer, P. D. *Nature* **1999**, *402*, 247. (c) Stock, D.; Leslie, A. G. W.; Walker, J. E. *Science* **1999**, *286*, 1700.
- (8) (a) Namba, K.; Vonderviszt, F. *Q. Rev. Biophys.* **1977**, *30*, 1. (b) Berg, H. C. *Annu. Rev. Biochem.* **2003**, *72*, 19.
- (9) Colbran, R. J. *Biochem. J.* **2004**, *378*, 1.
- (10) (a) Saibil, H. R.; Ranson, N. A. *Trends Biochem. Sci.* **2002**, *27*, 627. (b) Braig, K.; Otwinowski, Z.; Hedge, R.; Boisvert, D. C.; Joachimiak, A.; Horwich, A. L.; Sigler, P. B. *Nature* **1994**, *371*, 578. (c) Wang, J.; Boisvert, D. C. *J. Mol. Biol.* **2003**, *327*, 843.

sis. Despite this interest, the number of examples in which oriented molecular motions have been identified in small molecules is still not great.

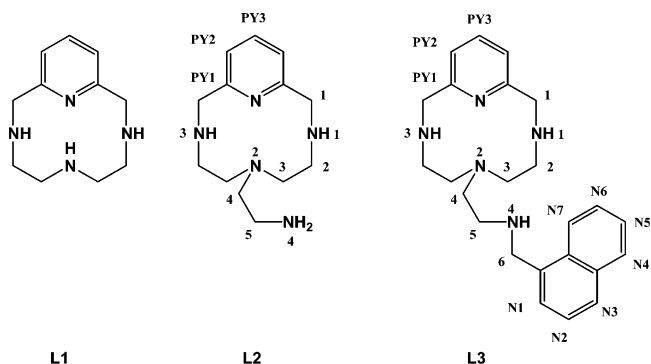
To have molecules able to perform controlled motions, several strategies can be approached. One of them consists of introducing different binding units in noncovalently interlocked or threaded molecules. In such systems, changes in a chemical or physical input can drive movements of the guest species between the different binding sites or slippage or gliding motions of one of the interlocked or threaded molecules with respect to the others. Rotaxanes and catenanes represent classical examples in this respect.¹² Recently, a very imaginative molecule able to contract its size in response to a redox impulse has been reported and termed as a “molecular muscle” for its resemblance to the movement exerted by striate muscles.¹³

Another strategy will be to join covalently within the same molecule a rigid and a flexible moiety so that the flexible one changes its position with respect to the rigid one responding to a given input that can be of chemical or physical nature.

Polyamines consisting of a “fixed” macrocyclic core appended with an arm containing additional amine donor groups belong to this category and were prepared by Lotz and Kaden for the first time.¹⁴ Later, Fabbrizzi et al.¹⁵ coined the term “scorpionate” for these molecules since the pendant arm could somehow represent the tail of the scorpion that folds to bind the metal ion encircled by the macrocycle. However, on acidification, the amino group in the arm protonates and moves apart from the metal site because of electrostatic reasons.¹⁵ This molecular motion has been further signaled by the introduction of fluorophoric groups in the pendant arm whose fluorescence changed depending on whether the donor atom in the tail was coordinated or not.¹⁶ Ni²⁺ complexes of scorpionands have also been prepared using the own metal as a template of the reaction of condensation of the amine tris(2-aminoethyl)amine (tren) and a dialdehyde.¹⁷ More recently, Bianchi et al. have reported on a phenanthrolinephane azamacrocyclic Zn²⁺ complex with a tail containing an anthracene group showing

additional π - π -stacking interactions between the phenanthroline and anthracene rings when the nitrogen atom in the arm coordinates the metal ion.¹⁸

Herewith, we describe the preparation of the two new scorpionand compounds **L2** and **L3** (see Ligand Drawing). **L2** consists of a tren amine with two of its arms cyclized with 2,6-bis(bromomethyl)pyridine. In **L3**, the remaining pendant arm has been further functionalized with a fluorophoric naphthalene group. Additionally, we have re-prepared for comparative purposes pyridinophane **L1** that was first synthesized by H. Stetter et al.¹⁹ and further studied by Costa and Delgado.²⁰ We show by a variety of methods that the pH-driven movement that performs in **L2** and **L3** the pendant arm function to bind or unbind the metal ion (Cu²⁺ in this work) can also be achieved in the absence of any metal ion. This behavior, which has not been reported previously for other scorpionand ligands, is powered by the formation of intramolecular hydrogen bonds between the amino group in the arm and those in the macrocyclic core, with additional contributions from π - π -stacking interactions between the naphthalene and pyridine rings. Additionally, we provide a kinetic study on the complexation and decomplexation of Cu²⁺ by **L2** and **L3** that furnishes additional information about the dynamics of these systems.



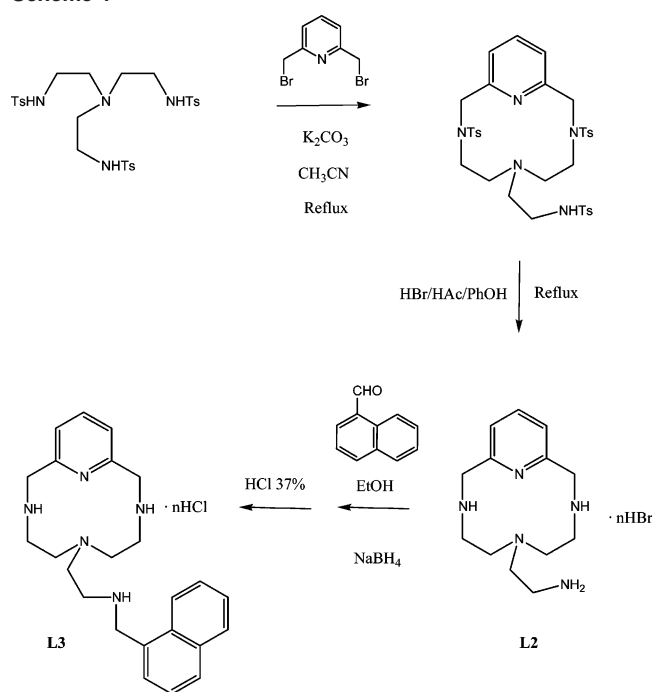
Results and Discussion

Synthesis of L2 and L3. The synthesis of the ligands **L2** and **L3** was achieved following a modification of the Richman–Atkins procedure²¹ by reaction of the pertosylated polyamine tren with 2,6-bis(bromomethyl)pyridine in 1:1 molar ratio using K₂CO₃ as a base in refluxing CH₃CN (Scheme 1). Similar procedures have been used for the preparation of azacyclophanes²² and more recently for the preparation of a phenanthrolinephane scorpionand with an anthracene pendant unit.¹⁷ Detosylation is carried out with

- (11) Rossmann, M. G.; Mesyanzhinov, V. V.; Arisaka, F.; Leiman, P. G. *Curr. Opin. Struct. Biol.* **2004**, *14*, 171.
 (12) (a) Dietrich-Buchecker, C. O.; Sauvage, J. P.; Kintzinger, J. P. *Tetrahedron Lett.* **1983**, *24*, 5095. (b) Cesario, M.; Dietrich-Buchecker, C. O.; Guilhem, J.; Pascard, C.; Sauvage, J. P. *J. Chem. Soc., Chem. Commun.* **1985**, 244. (c) Raehm, L.; Sauvage, J.-P. *Struct. Bonding (Berlin)* **2001**, *99*, 55. (d) Balzani, V.; Credi, A.; Venturi, M. *Molecular Devices and Machines. A Journey into the Nanoworld*; Wiley-VCH: Weinheim, Germany, 2003.
 (13) (a) Jiménez, M. C.; Dietrich-Buchecker, C.; Sauvage, J.-P. *Angew. Chem., Int. Ed.* **2000**, *39*, 3284. (b) Jiménez, M. C.; Dietrich-Buchecker, C.; Sauvage, J.-P. *Chem.—Eur. J.* **2002**, *8*, 1456. (c) Jiménez, M. C.; Dietrich-Buchecker, C.; Sauvage, J.-P. *Chem. Commun.* **2003**, 1613.
 (14) Lotz, T. J.; Kaden, T. A. *J. Chem. Soc., Chem. Commun.* **1977**, 15.
 (15) Pallavicini, P. S.; Perotti, A.; Poggi, A.; Segui, B.; Fabbrizzi, L. *J. Am. Chem. Soc.* **1987**, *109*, 5139.
 (16) Amendola, V.; Fabbrizzi, L.; Lichelli, M.; Mangano, C.; Pallavicini, P.; Parodi, L.; Poggi, A. *Coord. Chem. Rev.* **1999**, *192*, 649.
 (17) (a) Keypour, H.; Salehzadeh, S.; Pritchard, R. G.; Parish, R. V. *Inorg. Chem.* **2000**, *39*, 5787. (b) Herrera, A. M.; Staples, R. J.; Kryakov, S. V.; Nazarenko, A. Y.; Rybak-Akimova, E. V. *J. Chem. Soc., Dalton Trans.* **2003**, 846.

- (18) (a) Bencini, A.; Bianchi, A.; Lodeiro, C.; Masotti, A.; Parola, A. J.; Melo, J. S.; Pina, F.; Valtancoli, B. *Chem. Commun.* **2000**, 1639. (b) Bencini, A.; Berni, E.; Bianchi, A.; Fornasari, P.; Giorgi, C.; Lima, J. C.; Lodeiro, C.; Melo, M. J.; Seixas de Melo, J.; Parola, A. J.; Pina, F.; Pina, J.; Valtancoli, B. *J. Chem. Soc., Dalton Trans.* **2004**, 2180.
 (19) Stetter, H.; Frank, W.; Mertens, R. *Tetrahedron* **1981**, *32*, 5257.
 (20) Costa, J.; Delgado, R. *Inorg. Chem.* **1993**, *32*, 5257.
 (21) (a) Richman, J. E.; Atkins, T. J. *J. Am. Chem. Soc.* **1974**, *96*, 2228. (b) Richman, J. E.; Atkins, T. J.; Oettle, W. F. *Organic Synthesis*; Wiley & Sons: New York, 1988; pp 652, Vol. VI. (c) Shaw, B. L. *J. Am. Chem. Soc.* **1975**, *97*, 3856.

Scheme 1



HBr/HAc, and the final product is obtained as the hydrobromide salt.

Compound **L3** was obtained by reacting **L2** in its free-amine form with naphthalene-1-carbaldehyde in dry ethanol followed by in situ reaction with sodium borohydride and precipitation as a hydrochloride salt.

X-ray Diffraction Studies. Crystal Structure of [H(L3)]ClO₄·H₂O (1). Slow evaporation of an aqueous solution of **L3**·3HCl in an excess of NaClO₄ at pH = 9 led to the formation of crystals of formula [H(L3)]ClO₄·H₂O (**1**) that were suitable for X-ray analysis. The crystal structure of **1** consists of [H(L3)]⁺ cations, ClO₄⁻ anions, and water molecules (Figure 1). The most distinctive feature of **1** is the formation of an intramolecular hydrogen bond between the amine group in the arm and the protonated ammonium group in the macrocyclic core (N(1)–N(4) = 2.903 Å, N(1)–H···N(4) = 2.083 Å) (Figure 1).

The proton of the ammonium group was located from difference Fourier maps and successfully refined as an isotropic atom. The formation of this hydrogen bond folds the pendant arm toward the macrocycle so that a favorable π -stacking interaction between the naphthalene ring in the arm and the pyridine core is also produced. The angle between the planes of the aromatic fragments is 17.6°, and the distance between the centroids is 4.24 Å.

The different [H(L3)]⁺ units are interconnected, forming chains through an intermolecular hydrogen-bond network in which are involved both secondary amine groups in the

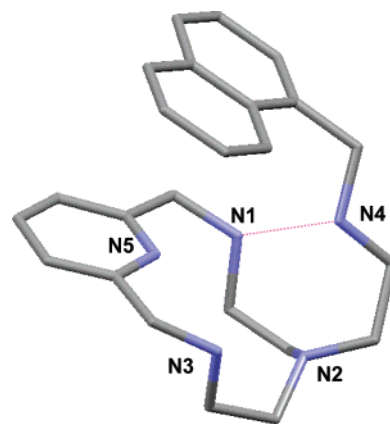


Figure 1. Stick drawing of the [H(L3)]⁺ cation.

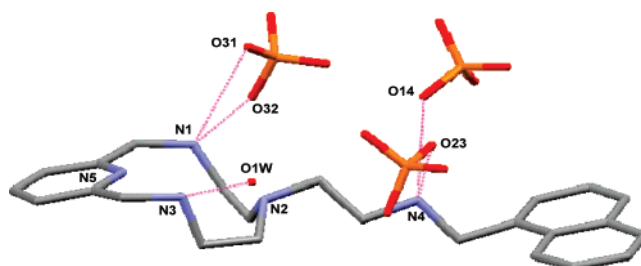


Figure 2. Stick representation of [H₃(L3)](H₂PO₄)₃·H₂O.

macrocyclic core, the water molecules, and the perchlorate anions (see Figure S1 in the Supporting Information). The water molecule links through hydrogen bonding the protonated amino group of a unit (N1) with the nonprotonated amino group of the following unit (N3). The distances are as follows: N(3)–O(1W) = 2.737 Å and O(1W)–N(1) = 2.738 Å. The different chains in the crystal structure are isolated and do not show any kind of interconnection.

Crystal Structure of [H₃(L3)](H₂PO₄)₃·H₂O (2). Slow evaporation of an aqueous solution of **L3**·3HCl and K₂HPO₄ at an initial pH = 4 in an excess of NaClO₄ led to the formation of crystals of [H₃(L3)](H₂PO₄)₃·H₂O (**2**). In this case, the structure consists of trivalent [H₃(L3)]³⁺ cations, monovalent H₂PO₄⁻ anions, and water molecules (Figure 2). The trivalent cations adopt an extended conformation in which the pendant-charged arm lies far from the discharged macrocyclic core in order to minimize electrostatic repulsions between same-side charges. Consequently, in this case, unlike that of the previous structure, there is no intramolecular hydrogen bonding or π - π stacking.

Although the hydrogen atoms of the dihydrogenphosphate moieties were located in calculated positions, these anions appear to be hydrogen bonded to two of the charged ammonium groups. The ammonium group of the arm would be forming hydrogen bonds with two oxygen atoms, each one belonging to a different dihydrogenphosphate moiety (N(4)–O(23) = 2.97 Å, N(4)–O(14) = 2.84 Å). One of the ammonium groups of the macrocyclic core would be hydrogen bonded to two oxygen atoms of the third dihydrogenphosphate unit present in the asymmetric unit (N(1)–O(31) = 3.00 Å, N(1)–O(32) = 3.05 Å), and the other ammonium group of the macrocyclic core would be hydrogen bonded to a water molecule (N3–O1W = 2.82 Å). Interest-

(22) (a) Bencini, A.; Burguete, M. I.; García-España, E.; Luis, S. V.; Miravet, J. F.; Soriano, C. *J. Org. Chem.* **1993**, *58*, 4749. (b) Aguilar, J. A.; García-España, E.; Guerrero, J. A.; Luis, S. V.; Llinares, J. M.; Ramírez, J. A.; Soriano, C. *Inorg. Chim. Acta* **1996**, *246*, 287. (c) Díaz, P.; Basallote, M. G.; Máñez, M. A.; García-España, E.; Gil, L.; Latorre, J.; Soriano, C.; Verdejo, B.; Luis, S. V. *J. Chem. Soc., Dalton Trans.* **2003**, 1186.

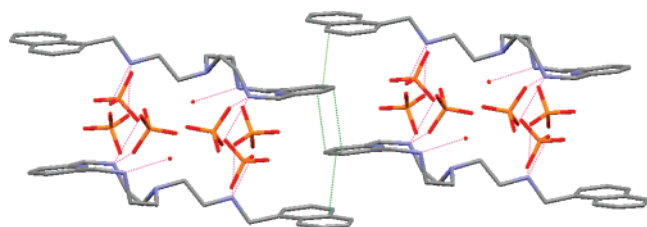


Figure 3. View of the crystal packing of **2** showing the stacking interactions between pyridine and naphthalene rings.

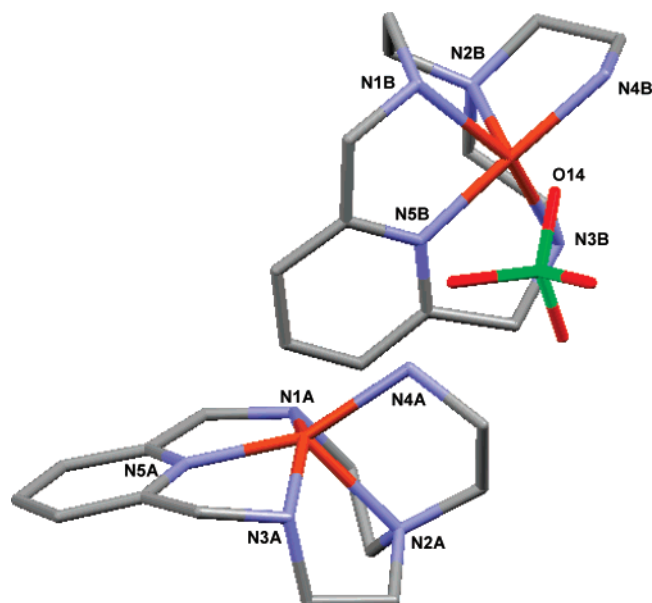


Figure 4. Stick representation of the two different $[\text{Cu}(\text{L}2)]^{2+}$ cations in the crystal structure of **3**. In unit B, the perchlorate pointing toward the metal ion is shown.

ingly enough, although the crystals evolve from a solution containing an excess of sodium perchlorate, the only counteranion present is dihydrogenphosphate. The $\text{H}_2\text{PO}_4^-/\text{L}3$ 3:1 stoichiometry found in the crystal does not agree with the solution studies in which a $\text{H}_2\text{PO}_4^-/\text{L}3$ 1:1 stoichiometry was inferred from either NMR spectroscopy or speciation studies.²³

Although there is no intramolecular π - π stacking, the structure shows intermolecular π - π stacking between pyridine and naphthalene moieties belonging to two different units (Figure 3). The distance between the naphthalene-pyridine separation is 3.455 Å with an angle of 7.2°, and the distance between the pyridine rings is 3.645 Å.

Crystal Structure of $[\text{Cu}(\text{L}2)(\text{ClO}_4)_2] \cdot \text{H}_2\text{O}$ (3**).** Slow evaporation of an aqueous solution of $\text{Cu}(\text{ClO}_4)_2 \cdot 6\text{H}_2\text{O}$ and $\text{L}2 \cdot 4\text{HBr}$ at an initial pH = 9 yields the precipitation of a crystalline compound of formula $[\text{Cu}(\text{L}2)(\text{ClO}_4)_2] \cdot \text{H}_2\text{O}$ (**3**). The asymmetric unit includes two different $[\text{Cu}(\text{L}2)]^{2+}$ cations, ClO_4^- anions, and water molecules (Figure 4). Selected bond angles and lengths are included in Table 1.

The Cu^{2+} coordination geometry in the two $[\text{Cu}(\text{L}2)]^{2+}$ cations is that of slightly distorted square-pyramidal type with

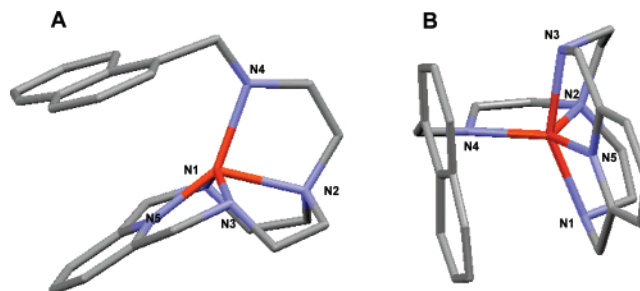


Figure 5. Representation of two views of the cation $[\text{Cu}(\text{L}3)]^{2+}$ showing the mixture of square-pyramidal and trigonal-bipyramidal dispositions.

Table 1. Selected Bond Lengths (Å) and Angles (deg) for Compound **3**

Bond Distances			
Cu(1)–N(1A)	2.074(9)	Cu(2)–N(1B)	2.116(8)
Cu(1)–N(2A)	2.189(8)	Cu(2)–N(2B)	2.231(8)
Cu(1)–N(3A)	2.097(9)	Cu(2)–N(3B)	2.104(8)
Cu(1)–N(4A)	2.052(9)	Cu(2)–N(4B)	1.997(8)
Cu(1)–N(5A)	1.950(9)	Cu(2)–N(5B)	1.938(8)
		Cu(2)–O(14)	2.635(8)
Bond Angles			
N(1A)–Cu(1)–N(2A)	83.3(3)	N(1B)–Cu(2)–N(2B)	82.5(3)
N(1A)–Cu(1)–N(4A)	103.5(4)	N(1B)–Cu(2)–N(4B)	99.7(3)
N(1A)–Cu(1)–N(5A)	81.0(4)	N(1B)–Cu(2)–N(5B)	81.5(3)
N(2A)–Cu(1)–N(3A)	84.7(3)	N(2B)–Cu(2)–N(3B)	84.5(3)
N(2A)–Cu(1)–N(4A)	82.7(3)	N(2B)–Cu(2)–N(4B)	84.0(3)
N(2A)–Cu(1)–N(5A)	119.5(3)	N(2B)–Cu(2)–N(5B)	99.4(3)
N(3A)–Cu(1)–N(4A)	100.8(4)	N(3B)–Cu(2)–N(4B)	98.0(3)
N(3A)–Cu(1)–N(5A)	82.3(4)	N(3B)–Cu(2)–N(5B)	81.7(3)

the primary nitrogen atom in the tail occupying one of the equatorial positions; the remaining positions in the base of the pyramids are formed by the two secondary amine groups of the macrocyclic cores and the pyridine nitrogens, which have the shortest distance to the metal ($\text{Cu}(1)\text{--N}(5\text{A}) = 1.950(9)$ Å, $\text{Cu}(2)\text{--N}(5\text{B}) = 1.938(8)$ Å). The slightly elongated axial positions are occupied by the tertiary amino group. The Cu^{2+} ions lie nicely on the mean plane defined by the equatorial nitrogens with elevations of just 0.037 and 0.100 Å for Cu(1) and Cu(2), respectively. The distances and angles of the coordination spheres are collected in Table 1. In the $[\text{Cu}(\text{L}2)]^{2+}$ cation labeled as B, one oxygen atom of a perchlorate counteranion is pointing toward the metal in the direction of the remaining axial position of a very distorted octahedron ($\text{Cu}(2)\text{--O}(14) = 2.635$ Å). The location of the nitrogen atom of the amino group located opposite to the pyridine ring in the axial position of the square pyramid was already observed in one of the crystalline forms of the complex $[\text{Cu}(\text{L}1)\text{Br}](\text{ClO}_4)$.²⁴

Crystal Structure of $[\text{Cu}(\text{L}3)(\text{ClO}_4)_2]$ (4**).** Slow evaporation of an aqueous solution of $\text{Cu}(\text{ClO}_4)_2 \cdot 6\text{H}_2\text{O}$ and $\text{L}3 \cdot 3\text{HCl}$ at an initial pH = 9 gave crystals of formula $[\text{Cu}(\text{L}3)](\text{ClO}_4)_2$ (**4**) that were suitable for X-ray diffraction analysis. In this crystal structure, the coordination geometry around the Cu^{2+} ions is midway between a strongly distorted square pyramid and a trigonal bipyramid (Figure 5). The percentage of trigonal-bipyramidal units calculated by means of the facial

(23) Preliminary potentiometric studies carried out by ³¹P NMR and pH-metric titrations show the formation of phosphate–**L2** and phosphate–**L3** adducts of 1:1 stoichiometry in 0.15 mol·dm^{−3} NaClO₄ aqueous solution. These results will be discussed and published elsewhere.

(24) Felix, V.; Costa, J.; Delgado, R.; Drew, M. G. B.; Duarte, M. T.; Resende, C. J. *Chem. Soc., Dalton Trans.* **2001**, 1462.

Table 2. Selected Bond Length (Å) and Angles (deg) for Compound 4

bond distances		bond angles	
Cu(1)–N(1)	2.082(10)	N(1)–Cu(1)–N(2)	85.1(5)
Cu(1)–N(2)	2.106(9)	N(1)–Cu(1)–N(4)	105.1(4)
Cu(1)–N(3)	2.034(9)	N(1)–Cu(1)–N(5)	80.4(4)
Cu(1)–N(4)	2.063(9)	N(2)–Cu(1)–N(3)	86.3(4)
Cu(1)–N(5)	1.923(8)	N(2)–Cu(1)–N(4)	83.3(5)
		N(2)–Cu(1)–N(5)	129.2(4)
		N(3)–Cu(1)–N(4)	103.1(4)
		N(3)–Cu(1)–N(5)	82.5(4)

Table 3. Logarithms of the Stepwise Protonation Constants for L1–L3 Determined in 0.15 mol·dm⁻³ NaClO₄ at 298.1 K

reaction ^a	L1	L2	L3
H + L ⇌ HL	10.54(1) ^b	10.20(6)	10.01(1)
H + HL ⇌ H ₂ L	7.96(1)	9.18(3)	8.71(1)
H + H ₂ L ⇌ H ₃ L	1.90(1)	7.84(4)	7.26(1)

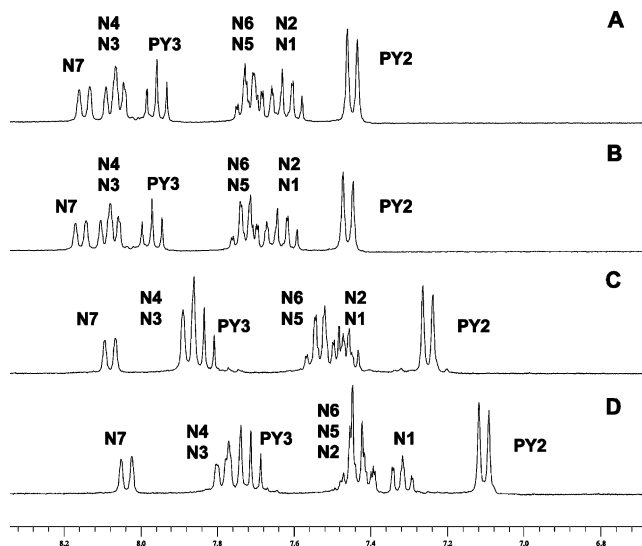
^a Charges omitted. ^b Values in parentheses are standard deviations in the last significant figure.

planes is 35%.²⁵ The equatorial positions in the square pyramid will be occupied by the pyridine nitrogen atom, the secondary nitrogen atoms in the macrocyclic core, and the secondary amino group in the tail. The elevation of the Cu²⁺ atom over the mean plane defined by the nitrogen atoms is 0.12 Å. The axial position will be occupied by the nitrogen atom of the tertiary amino group; however, in this case the axial position would be practically undistorted (Cu(1)–N(2) = 2.106(9) Å) (see Figure 5A). Selected bond distances and angles are included in Table 2. In the case where the structure is defined as a trigonal bipyramid, then the equatorial plane will be occupied by the pyridine nitrogen, the tertiary amino group of the macrocyclic core, and the secondary amino group of the arm. The axial positions will involve the two secondary amino groups of the macrocycle (see Figure 5B).

One of the most relevant aspects in this structure is the π – π stacking that occurs between the pyridine and naphthalene rings following the coordination of the metal ion. The distance between the centroid of the pyridine ring and the naphthalene plane is 3.852 Å, and the mean angle between the aromatic planes is 13.2°. A similar situation has been described for a Zn²⁺ complex of an azaphenanthroline having anthracene as a pendant arm.¹⁸

Molecular Rearrangements in Solution. pH-Driven Molecular Rearrangements in the Absence of Cu²⁺. To ascertain if the molecular rearrangement, in which the pendant arm approaches or leaves the macrocyclic core as a result of a change in the protonation state, also occurs in solution, we have carried out several studies on these systems. First, the protonation constants for both systems were measured by pH-metric titrations in 0.15 mol·dm⁻³ NaClO₄ aqueous solution at 298.1 K. The protonation constants for L2 and L3 are collected in Table 3 along with those determined for L1 under the same conditions. These latter constants agree very well with those reported previously by Costa and Delgado at a different ionic strength.²⁰

Both L2 and L3 present in the pH range of study (2.5–11.0) three stepwise protonation constants separated by ca.

**Figure 6.** ¹H NMR spectra in D₂O of L3 recorded at (A) pD = 1.6; (B) pD = 4.1; (C) pD = 8.2; (D) pD = 9.4.

1.3 logarithmic units. In neither of these two ligands has it been possible to measure by pH-metric titrations a fourth protonation constant. This last protonation step should involve the central tertiary amino nitrogen of the macrocyclic ring and should have a very low value since it will imply electrostatic repulsion with three charged polyammonium groups each separated by an ethylenic chain. On the other hand, as is well-known, tertiary nitrogens are less basic in aqueous solution than primary and secondary ones and this will contribute even more to the reduction in the basicity of this group.^{26–29} It is interesting to note that the protonation constants of the three detected steps are lower for L3 than for L2, which can be ascribed to the hydrophobic environment generated by the naphthalene substituent that disfavors the solvation of the amino groups.²⁶

L3, due to the presence of the naphthalene ring, is a molecule particularly well-suited for the spectroscopic detection of molecular reorganizations in solution. First, as seen in the crystal structure of 1, the bending of the arm leads to π – π stacking between the naphthalene and pyridine rings. In this respect, the ¹H NMR spectra recorded at variable pH show that on going from a pH level of 6 to 8, corresponding with the deprotonation of [H₃L3]³⁺ to give [H₂L3]²⁺, there is an upfield shift of all the aromatic signals of both naphthalene and pyridine ¹H signals, denoting that stacking between them occurs (Figure 6).

This stacking is also evidenced by the changes in the UV–vis spectra. On going from acidic to basic pH, the band

(25) Muetterties, E. L.; Guggenberger, L. G. *J. Am. Chem. Soc.* **1974**, *96*, 1748.

(26) (a) Sarnesky, J. E.; Surprenant, H. L.; Molen, F. K.; Reiley, C. N. *Anal. Chem.* **1975**, *47*, 2116. (b) Bencini, A.; Bianchi, A.; García-España, E.; Micheloni, M.; Ramírez, J. A. *Coord. Chem. Rev.* **1998**, *188*, 97.
 (27) Albelda, M. T.; García-España, E.; Jiménez, H. R.; Llinares, J. M.; Soriano, C.; Sornosa-Ten, A.; Verdejo, B. *Dalton Trans.* **2006**, 4474.
 (28) (a) Frassinetti, C.; Ghelli, S.; Gans, P.; Sabatini, A.; Moruzzi, M. S.; Vacca, A. *Anal. Biochem.* **1995**, *231*, 374. (b) Frassinetti, C.; Alderighi, L.; Gans, P.; Sabatini, A.; Vacca, A. *Anal. Bioanal. Chem.* **2003**, 376, 1041.
 (29) (a) Dagnall, S. P.; Hague, D. N.; McAdam, M. E.; Moreton, A. D. *J. Chem. Soc., Faraday Trans.* **1985**, *81*, 1483. (b) Hague, D. N.; Moreton, A. D. *J. Chem. Soc., Perkin Trans.* **1994**, *2*, 265.

centered at 220 nm that can be ascribed to a $\pi-\pi^*$ transition in the naphthalene ring experiences a decrease in intensity. However, above pH 6, the opposite behavior occurs and an increase in intensity is observed that can be ascribed to a charge-transfer band associated with the $\pi-\pi$ stacking of the aromatic rings (Figure S2 in the Supporting Information). In turn, the fluorescence emission spectra show a quenching effect when passing from $[\text{H}_3\text{L3}]^{3+}$ to $[\text{H}_2\text{L3}]^{2+}$, denoting that deprotonation of the secondary amino group closest to the naphthalene fragment is occurring at this stage (Figure S3 in the Supporting Information). This deprotonation makes operative a photoinduced electron transfer from the amine to the excited fluorophore, yielding a quenching of the fluorescence. Nevertheless, differing from other studied systems, in this case the observed quenching of the fluorescence is just partial. This incomplete quenching of the fluorescence could be explained if the hydrogen bonding observed in the solid state would also persist in solution. Hydrogen bonding between the amino group in the arm and the protonated secondary amino groups in the macrocyclic core would somehow block the electron pair of the amine group of the arm, preventing its full transfer to the excited fluorophore, hence, leaving a residual emission.

The existence of hydrogen bonding is also supported by the ^1H and ^{13}C NMR spectra recorded at variable pH for this system. Despite what is usually observed for other polyamine compounds with ethylene bridges separating the nitrogen atoms, the variations of the ^1H NMR and ^{13}C NMR signals are not very conclusive about the protonation of determined nitrogens in the molecule. It is well-established that upon protonation the carbon atom in β position and the hydrogen nuclei attached to the carbon atom in α position to the nitrogens are those exhibiting, respectively, the largest upfield and downfield changes in their chemical shifts.^{26–29} However, in this case, although all the ^1H signals move downfield and all the ^{13}C NMR signals move upfield on decreasing the pH, there are no distinctive shifts for any of them (see Table S1 and Figure S4 in the Supporting Information). This would support the tenet that in solution the first two protons are shared between the different nitrogen atoms in the receptor.

The analysis of the values of the protonation constants of **L2** and of the ^1H and ^{13}C NMR spectra of **L2** points to a similar situation (see Table S2 and Figures S4 and S5 in the Supporting Information). This is interesting since, as it is well-known, primary nitrogens are more basic in water than secondary and tertiary nitrogens due to solvation effects. However, in this case, the formation of hydrogen bonds between the amino group in the tail and those in the macrocycle alters this pattern and there is not a clear protonation sequence.

pH-Driven Molecular Rearrangements in the Presence of Cu^{2+} . Speciation Studies. pH-metric titrations carried out in $0.15 \text{ mol}\cdot\text{dm}^{-3} \text{ NaClO}_4$ at 298.1 K gave the stability constants and model species that are collected in Table 4 for the systems $\text{Cu}^{2+}-\text{L2}$ and $\text{Cu}^{2+}-\text{L3}$ along with those we have calculated under the same experimental conditions for the system $\text{Cu}^{2+}-\text{L1}$. Due to the slow kinetics of

Table 4. Logarithms of the Formation Constants of Cu^{2+} Complexes with **L2** and **L3** Determined in $0.15 \text{ mol}\cdot\text{dm}^{-3} \text{ NaClO}_4$ at 298.1 K

reaction ^a	L1	L2	L3
$\text{Cu} + \text{L} \rightleftharpoons \text{CuL}$	17.78(2) ^b	20.43(3)	19.65(4)
$\text{Cu} + \text{L} + \text{H} \rightleftharpoons \text{CuHL}$		24.28(2)	22.65(2)
$\text{CuL} + \text{H} \rightleftharpoons \text{CuHL}$		3.85(3)	3.00(2)
$\text{Cu} + \text{L} + \text{H}_2\text{O} \rightleftharpoons \text{CuL}(\text{OH}) + \text{H}$		-11.01(3)	

^a Charges omitted. ^b Values in parentheses are standard deviations in the last significant figure.

formation of the Cu^{2+} complexes, the interval between the successive additions of base was ca. 10 min for both systems $\text{Cu}^{2+}-\text{L2}$ and $\text{Cu}^{2+}-\text{L3}$. Moreover, in the case of **L3**, the measurements were checked by an out-of-cell batchwise procedure. In this procedure, several samples were prepared in separated flasks with different quantities of base, and then the attainment of the equilibrium was checked periodically following the variation in the electromotive force and in the visible spectra. Both procedures, direct and the batchwise, provided reproducible values of the stability constants.

The stability constants obtained for $[\text{Cu}(\text{L2})]^{2+}$ and $[\text{Cu}(\text{L3})]^{2+}$ are clearly higher than that obtained for the Cu^{2+} complex of the ligand **L1** without the pendant arm, also indicating that in solution the nitrogen atom of the arm is bound to the metal ion. The values for the protonation constant of the $[\text{Cu}(\text{L2})]^{2+}$ and $[\text{Cu}(\text{L3})]^{2+}$ complexes, which are much lower than the protonation constants of the free ligand, support the tenet that protonation of the nitrogen implies the breakage of a $\text{Cu}^{2+}-\text{N}$ bond.

Kinetic Studies. To obtain some information on the dynamics of the processes involving the dissociation of the metal ion and the movement of the pendant arm in the complexes with the **L2** and **L3** ligands, kinetic studies on the acid-promoted decomposition of the corresponding Cu^{2+} complexes were carried out. For this purpose, the equilibrium species distribution curves were used to determine the pH values at which solutions containing Cu^{2+} and the macrocycle in 1:1 molar ratio contain the corresponding $[\text{CuL}]^{2+}$ complexes as the major species. Solutions prepared under those conditions were then mixed in a stopped-flow instrument with an excess of acid, which causes decomposition of the complex according to eq 1, where H_xL^{x+} represents the protonated form of the ligand existing in the final solution. These kinds of studies have been recently shown to provide information not only on the complex decomposition itself but also on the existence of molecular movements in macrocyclic complexes.^{30,31} As the major goal of the kinetic studies was to analyze the behavior of the pendant arm during the course of the reaction, the unsubstituted **L1** macrocycle was also included for comparative purposes. As previously indicated, the synthesis of the latter macrocycle was reported some years ago by Stetter et al.¹⁹ and by Costa

(30) Mendoza, A.; Aguilar, J. A.; Basallote, M. G.; Gil, L.; Hernández, J. C.; Máñez, M. A.; García-España, E.; Ruiz-Ramírez, L.; Soriano, C.; Verdejo, B. *Chem. Commun.* **2003**, 3032.

(31) Aguilar, J.; Basallote, M. G.; Gil, L.; Hernández, J. C.; Máñez, M. A.; García-España, E.; Soriano, C.; Verdejo, B. *Dalton Trans.* **2004**, 94.

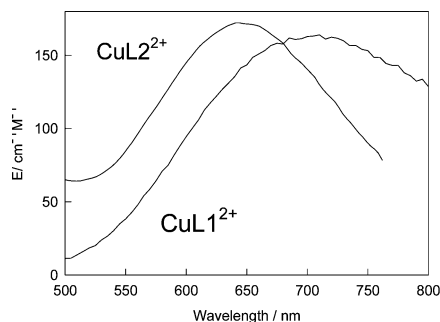


Figure 7. Electronic spectra for aqueous solutions containing the $[\text{Cu}(\text{L1})]^{2+}$ and $[\text{Cu}(\text{L2})]^{2+}$ complexes. The spectrum of the corresponding **L3** complex is similar to that of $[\text{Cu}(\text{L2})]^{2+}$.

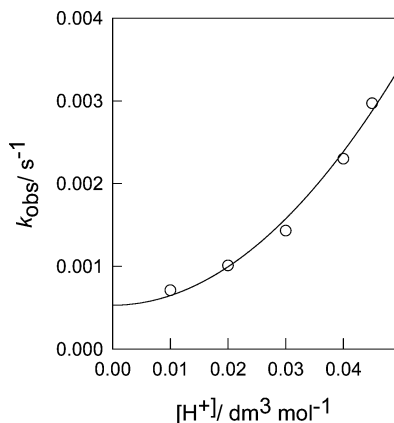
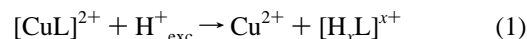


Figure 8. Plot of the dependence on the acid concentration of the observed rate constant for the acid-promoted decomposition of the $[\text{Cu}(\text{L1})]^{2+}$ complex ($[\text{NaClO}_4] = 0.15 \text{ mol} \cdot \text{dm}^{-3}$, 298.1 K).

and Delgado,²⁰ who also showed that the Cu^{2+} complex has a band at 695 nm in the UV–vis and EPR spectra indicative of a tetragonally elongated octahedral structure. We have also found that solutions containing the $[\text{Cu}(\text{L1})]^{2+}$ complex show a band centered at 695 nm (Figure 7), which disappears upon addition of the acid excess in a single kinetic step with rate constant k_{obs} showing an unusual dependence on the acid concentration (Figure 8). The experimental data can be satisfactorily fitted by eq 2 with $a = (5.2 \pm 0.9) \times 10^{-4} \text{ s}^{-1}$ and $b = 1.16 \pm 0.07 \text{ dm}^6 \cdot \text{mol}^{-2} \cdot \text{s}^{-1}$. Despite the large number of kinetic studies carried out on the decomposition of metal complexes with polydentate ligands, there are relatively few examples of processes showing a second-order dependence with respect to the acid concentration, although the acid-independent a term is usually absent.^{32–38} Decomposition of most Cu^{2+} complexes occurs with the rate law given in eq 3 or some of its simplified forms,³⁹ and the change to that in eq 2 indicates that the decomposition of

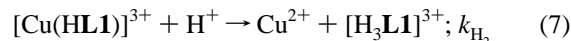
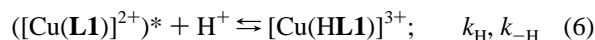
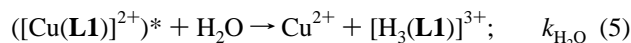
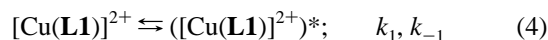
the complex requires the participation of one additional proton before the rate-determining step.



$$k_{\text{obs}} = a + b[\text{H}^+]^2 \quad (2)$$

$$k_{\text{obs}} = \frac{c + d[\text{H}^+]}{1 + e[\text{H}^+]} \quad (3)$$

The rate law in eq 2 can be explained with the mechanism in eqs 4–7, which has been slightly modified from the widely accepted formulation^{30,31,35,40} to account for the second-order dependence. In this mechanism, there is first the partial dissociation of one Cu–N bond to yield an activated intermediate $([\text{Cu}(\text{L1})]^{2+})^*$ (eq 4) that can decompose through two parallel pathways, one of them involving solvent attack (eq 5) and the other one two successive H^+ attacks (eqs 6–7). The rate law for this mechanism is given by eq 8 when the reaction intermediates are considered to be formed under steady-state conditions and $[\text{Cu}(\text{HL1})]^{3+}$ evolves to the parent $([\text{Cu}(\text{L1})]^{2+})^*$ species faster than to the reaction products ($k_{-\text{H}} \gg k_{\text{H}_2}[\text{H}^+]$). Further simplification to obtain a rate law (eq 9) equivalent to the experimental one (eq 2) can be achieved if $k_{-\text{H}}(k_{-1} + k_{\text{H}_2\text{O}}) \gg k_{\text{H}}k_{\text{H}_2}[\text{H}^+]^2$, an approximation that is also justified when both intermediates are considered to revert very rapidly to their parent species. For most polyamine complexes, the protonation processes following the breaking of the first Cu–N bond through the $k_{\text{H}_2\text{O}}$ and k_{H} pathways are very fast, so the second-order dependence on $[\text{H}^+]$ found for the decomposition of $[\text{Cu}(\text{L1})]^{2+}$ reflects a change in the rate-determining step for the acid-assisted decomposition pathway to proton attack at the second Cu–N bond.



$$k_{\text{obs}} = \frac{k_1 k_{\text{H}_2\text{O}} k_{-\text{H}} + k_1 k_{\text{H}} k_{\text{H}_2} [\text{H}^+]^2}{k_{-\text{H}}(k_{-1} + k_{\text{H}_2\text{O}}) + k_{\text{H}} k_{\text{H}_2} [\text{H}^+]^2} \quad (8)$$

$$k_{\text{obs}} = \frac{k_1 k_{\text{H}_2\text{O}} k_{-\text{H}} + k_1 k_{\text{H}} k_{\text{H}_2} [\text{H}^+]^2}{k_{-\text{H}}(k_{-1} + k_{\text{H}_2\text{O}})} \quad (9)$$

As expected from the different coordination environment of the metal ion, the spectra of the $[\text{Cu}(\text{L2})]^{2+}$ and $[\text{Cu}(\text{L3})]^{2+}$ species (Figure 7) are significantly different from that of the corresponding **L1** complex, the absorption maximum now being located at 645 nm; i.e., the band is shifted 50 nm to higher energies as a consequence of the coordination of the

- (32) Hay, R. W.; Bembi, R.; Moodie, W. T.; Norman, P. R. *J. Chem. Soc., Dalton Trans.* **1982**, 2131.
 (33) Hay, R. W.; Pujari, M. P.; McLaren, F. *Inorg. Chem.* **1984**, 23, 3033.
 (34) Curtis, N. F.; Osvath, S. R. *Inorg. Chem.* **1988**, 27, 305.
 (35) Lan, W. J. L.; Chung, C. S. *J. Chem. Soc., Dalton Trans.* **1994**, 191.
 (36) Hay, R. W.; Tarafder, M. T. H.; Hassan, M. M. *Polyhedron* **1996**, 15, 725.
 (37) De Santis, G.; Fabbri, L.; Perotti, A.; Sardone, N.; Taglietti, A. *Inorg. Chem.* **1997**, 36, 1998.
 (38) Basallote, M. G.; Durán, J.; Fernández-Tujillo, M. J.; Máñez, M. A. *J. Chem. Soc., Dalton Trans.* **2002**, 2074.
 (39) Basallote, M. G.; Durán, J.; Fernández-Trujillo, M. J.; Máñez, M. A. *J. Chem. Soc. Dalton Trans.* **1999**, 3817 and references therein.

- (40) Chen, L. H.; Chung, C. S. *Inorg. Chem.* **1989**, 28, 1402.

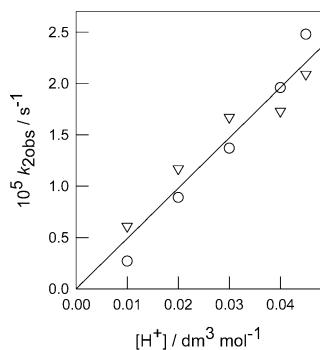
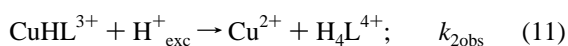
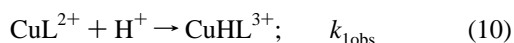


Figure 9. Plot of the dependence on the acid concentration of the observed rate constant for the second kinetic step in the acid-promoted decomposition of the $[\text{Cu}(\text{L}2)]^{2+}$ (circles) and $[\text{Cu}(\text{L}3)]^{2+}$ (triangles) complexes ($[\text{NaClO}_4] = 0.15 \text{ mol}\cdot\text{dm}^{-3}$, 298.1 K). For simplicity, only the line corresponding to the best fit of the whole set of data for both complexes is shown. For both complexes, there is a first step that occurs within the mixing time of the stopped-flow instrument.

pendant arm of the **L2** or **L3** ligands. However, when solutions of $[\text{Cu}(\text{L}2)]^{2+}$ or $[\text{Cu}(\text{L}3)]^{2+}$ are mixed in the stopped-flow instrument with an excess of acid, the spectrum recorded immediately upon mixing shows a band centered at 690 nm whose intensity decreases so slowly that the kinetics of the process had to be studied using conventional UV–vis spectrophotometry. These results demonstrate that decomposition of the $[\text{Cu}(\text{L}2)]^{2+}$ and $[\text{Cu}(\text{L}3)]^{2+}$ species occurs with biphasic kinetics (eqs 10–11 with $\text{L} = \text{L}2, \text{L}3$). The first step is too fast for its rate constant ($k_{1\text{obs}}$) to be measured even with the stopped-flow technique (mixing time of ca. 1.7 ms for the instrument used), and it leads to the formation of $[\text{Cu}(\text{HL}2)]^{3+}$ and $[\text{Cu}(\text{HL}3)]^{3+}$ intermediates with absorption spectra similar to that of the $[\text{Cu}(\text{L}1)]^{2+}$ complex, which indicates that dissociation of the amino group in the pendant arm is extremely rapid and is signaled by a measurable shift in the absorption spectrum. The second step leads to complete decomposition of the complex, and the spectral changes can be fitted satisfactorily by a single exponential to obtain $k_{2\text{obs}}$ values that show a linear dependence with respect to the acid concentration (eq 12; see Figure 9). The values of c are $(3 \pm 2) \times 10^{-5} \text{ s}^{-1}$ for the **L3** complex and negligible for the **L2** complex, whereas the values derived for d are $(5.0 \pm 0.3) \times 10^{-4} \text{ dm}^3 \text{ mol}^{-1} \text{ s}^{-1}$ ($[\text{Cu}(\text{HL}2)]^{3+}$) and $(3.9 \pm 0.5) \times 10^{-4} \text{ dm}^3 \text{ mol}^{-1} \text{ s}^{-1}$ ($[\text{Cu}(\text{HL}3)]^{3+}$). These values and the plot in Figure 9 indicate that the kinetics of decomposition of both species are quite similar and, actually, a satisfactory fit can be obtained by the joined fit of the data for both complexes, which yields $d = (4.9 \pm 0.2) \times 10^{-4} \text{ dm}^3 \text{ mol}^{-1} \text{ s}^{-1}$ and a negligible value of c .



$$k_{2\text{obs}} = c + d[\text{H}^+] \quad (12)$$

The experimental rate law for the decomposition of the $[\text{Cu}(\text{HL})]^{3+}$ intermediates generated during the decomposition of the complexes with the **L2** and **L3** macrocycles is a

simplification of the widely observed one (eq 3), which can be rationalized with the mechanism in eqs 4–7, although in this case the $[\text{Cu}(\text{H}_2\text{L})]^{3+}$ species formed by H^+ attack to the activated ($[\text{Cu}(\text{HL})]^{3+}$)* intermediate is converted very rapidly to the final products, as observed for the decomposition of most polyamine Cu^{2+} complexes. In that case, the rate law is given by eq 13 and reduces to the same form as that of eq 12 when $k_{-1} + k_{\text{H}_2\text{O}} \gg k_{\text{H}}[\text{H}^+]$. As the experimentally available kinetic parameters (c , d) are complex combinations of the mechanistically relevant rate constants (k_1 , k_{-1} , $k_{\text{H}_2\text{O}}$, k_{H}), they provide little information about the intimate mechanism of the decomposition process. However, the relative values of c and d found for the $[\text{Cu}(\text{HL}2)]^{3+}$ and $[\text{Cu}(\text{HL}3)]^{3+}$ complexes indicate that they decompose almost exclusively through the proton-assisted pathway; i.e., H_2O is not able to cause the complete breakage of the activated Cu–N bond in the corresponding ($[\text{Cu}(\text{HL})]^{3+}$)* intermediates. The absence of significant contributions from the solvent-assisted pathway is quite common in polyamine complexes with five-membered chelate rings, the relevance of this pathway being greater when the complex contains some six-membered rings.⁴⁰

$$k_{\text{obs}} = \frac{k_1 k_{\text{H}_2\text{O}} + k_1 k_{\text{H}}[\text{H}^+]}{k_{-1} + k_{\text{H}_2\text{O}} + k_{\text{H}}[\text{H}^+]} \quad (13)$$

It is interesting to note that the kinetics of decomposition of the $[\text{Cu}(\text{HL}2)]^{3+}$ and $[\text{Cu}(\text{HL}3)]^{3+}$ intermediates is different from that of $[\text{Cu}(\text{L}1)]^{2+}$ despite the similarity of the electronic spectra of the three species. The observed rate constants are 2 orders of magnitude slower for the **L2** and **L3** complexes, and the rate law changes from second to first-order dependence with respect to the acid concentration. Although the observation of different kinetics of decomposition for species with similar coordination environments for the metal ion can be considered surprising at first sight, we have previously found³² that the observation of kinetic changes associated with minor changes in the structure of the complexes is quite common in the decomposition of macrocyclic Cu^{2+} complexes because the rate of decomposition is strongly dependent on the structural distortions, the lability of the Cu–N bonds increasing with strain.⁴⁰ In the present case, the kinetic results seem to indicate that the structures of the $[\text{Cu}(\text{HL}2)]^{3+}$ and $[\text{Cu}(\text{HL}3)]^{3+}$ species are very similar to each other but significantly different from that of $[\text{Cu}(\text{L}1)]^{2+}$, the origin of the different strain probably associated with the presence or absence of the uncoordinated pendant arm.

A different behavior of the **L2** and **L3** ligands with respect to **L1** was also observed in the kinetics of formation of their Cu^{2+} complexes. To make complex formation slow enough to be measured with the stopped-flow instrument, kinetic studies on complex formation had to be carried out under non-pseudo first-order conditions, i.e., using stoichiometric concentrations of the metal ion and the ligand, and in moderately acidic media (pH = 3–5). Under these conditions, Cu^{2+} exists exclusively as the aqua complex and the

kinetic data are not complicated by any contribution from the hydroxo complexes to the rate of reaction. On the other hand, at low pH the ligands are highly protonated and this makes the equilibrium constants for the formation of the outer-sphere complexes with the metal ion small enough to allow kinetic studies on the formation of $\text{Cu}^{2+}\text{-L}$ complexes. As there is previous evidence⁴¹ that the addition of buffering agents leads to interactions with either the metal ion or the highly protonated macrocyclic species, the kinetics were studied in the absence of any buffer. Although this allows for significant changes in the H^+ concentration during complex formation, the kinetic data were still well behaved and this led to interesting conclusions on the behavior of these complexes.

For all three ligands, experiments carried out using the diode-array detector allowed the observation of spectral changes typical for complex formation according to eq 14. In all cases, the reaction occurs in a single step and the final spectra agree well with those expected from the species distribution curves calculated for the experimental conditions used in the kinetic experiments. Thus, for the case of the **L1** and **L3** ligands, the final spectra show the maximum typical for the corresponding $[\text{CuL}]^{2+}$ species centered at ca. 695 and 645 nm, respectively. For the case of **L2**, the final spectra show a broad band centered at 680 nm, in agreement with the expected formation of a mixture of $[\text{Cu}(\text{L2})]^{2+}$ and $[\text{Cu}(\text{HL2})]^{3+}$, the latter being the major species in acidic solutions.



With regard to the value of the second-order rate constant k , it was found to be independent of the value of the starting pH for the formation of the $[\text{Cu}(\text{L2})]^{2+}$ complex, its numerical value ($k = 0.18 \pm 0.02 \text{ M}^{-1} \text{ s}^{-1}$) being close to those reported for Cu^{2+} complex formation with the highly protonated forms of related ligands.^{42–46} As **L2** does not show any protonation process in the pH range covered in the kinetic studies, where it exists exclusively as $[\text{H}_3(\text{L2})]^{3+}$, it can be concluded that the measured value of k corresponds to complex formation between this species and Cu^{2+} . The small value of k suggests that none of the four nitrogen donors of the ligand has its lone electron pair readily available for complex formation, as previously revealed by the ligand protonation studies. In contrast, the rate of formation of the Cu^{2+} complexes with the ligands **L1** and **L3** shows a clear dependence on the pH that is illustrated in Figure 10 for the case of **L3**. The second-order rate constants

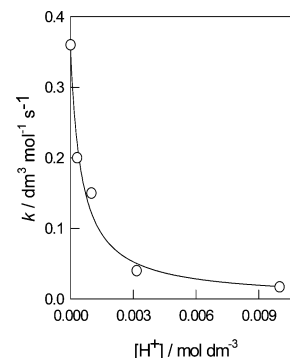


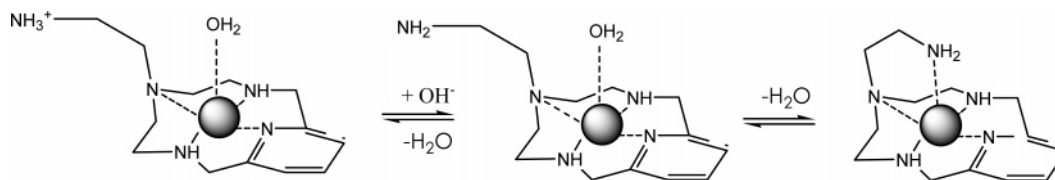
Figure 10. Plot of the dependence on the acid concentration of the observed rate constant for the formation of the $[\text{Cu}(\text{L3})]^{2+}$ complex at 298.1 K in the presence of $0.15 \text{ mol}\cdot\text{dm}^{-3} \text{ NaClO}_4$.

k for complex formation with both ligands change with the proton concentration according to eq 15 with values of $a = (1.1 \pm 0.4) \times 10^2 \text{ M}^{-1} \text{ s}^{-1}$ and $b = (1.2 \pm 0.5) \times 10^3 \text{ M}^{-1}$ for **L1** and $a = 0.36 \pm 0.02 \text{ M}^{-1} \text{ s}^{-1}$ and $b = (1.9 \pm 0.4) \times 10^3 \text{ M}^{-1}$ for **L3**. This rate law can be easily explained with the mechanism in eqs 16 and 17, which includes a rapid pre-equilibrium of protonation for the ligand, the most protonated form being ineffective for complex formation. The rate law for this mechanism coincides with eq 15 with the equivalencies $a = k_{\text{Cu}}$ and $b = K_{\text{H}}$. For the case of **L1**, the protonation process corresponds to the formation of $[\text{H}_3\text{L1}]^{3+}$ from $[\text{H}_2\text{L1}]^{2+}$ ($x = 2$), whereas k_{Cu} is the rate constant for complex formation between Cu^{2+} and $[\text{H}_2\text{L1}]^{2+}$. Analogously, K_{H} for **L3** corresponds to the equilibrium constant for the conversion of $[\text{H}_3\text{L3}]^{3+}$ to $[\text{H}_4\text{L3}]^{4+}$, and k_{Cu} is the rate constant for complex formation between Cu^{2+} and $[\text{H}_3\text{L3}]^{3+}$. It is interesting to note that for both ligands, the K_{H} values derived from the kinetic data are about 1 order of magnitude higher than those obtained from the potentiometric titrations. Nevertheless, the absence of buffering agent in the kinetic experiments leads to an increase in $[\text{H}^+]$ during the experiments that must result in a change in the apparent values derived for the protonation constant, so the agreement between the values can be considered satisfactory. It is also interesting to note that the k_{Cu} values for the formation of complexes with the $[\text{H}_3\text{L}]^{3+}$ forms of **L2** and **L3** are quite close to each other, which indicates that the effect of the naphthyl group on the kinetics of complex formation is negligible. In contrast, the rate constant for complex formation with $[\text{H}_2\text{L1}]^{2+}$ is almost 3 orders of magnitude higher. Although this can be caused, at least in part, by a favorable contribution from the change in the charge of the active ligand species, the participation of the amino group of the pendant arm in the network of hydrogen bonds, revealed in the NMR studies of ligand protonation, hinders the formation of outer-sphere complexes with the conformation required for metal coordination and surely contributes also to the decreased rate of complexation with the $[\text{H}_3\text{L}]^{3+}$ forms of **L2** and **L3**.

As a summary, the kinetic data indicate that the formation of a network of hydrogen bonds with the participation of all the donor atoms makes the reaction with the $[\text{H}_n\text{L}]^{n+}$ species slower than expected on the basis of their charge and the lability of the metal center, the effect being more pronounced

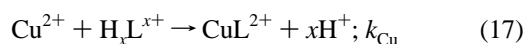
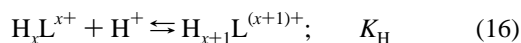
- (41) Basallote, M. G.; Durán, J.; Fernández-Trujillo, M. J.; Máñez, M. A.; Szpoganicz, B. *J. Chem. Soc., Dalton Trans.* **1999**, 1093.
 (42) Soibinet, M.; Gusmeroli, D.; Siegfried, L.; Kaden, T. A.; Palivan, C.; Schweiger, A. *J. Chem. Soc., Dalton Trans.* **2005**, 2138.
 (43) Westerby, B. C.; Juntunen, K. L.; Leggett, G. H.; Pett, V. B.; Koenigbauer, M. J.; Purgett, M. D.; Taschner, M. J.; Ochrymowicz, L. A.; Rorabacher, D. B. *Inorg. Chem.* **1991**, *30*, 2109.
 (44) Biver, T.; Lombardi, D.; Secco, F.; Tiné, M. R.; Venturini, M.; Bencini, A.; Bianchi, A.; Valtancoli, B. *J. Chem. Soc., Dalton Trans.* **2006**, 1524.
 (45) Biver, T.; Secco, F.; Tiné, M. R.; Venturini, M. *J. Inorg. Biochem.* **2004**, *98*, 33.
 (46) Siegfried, L.; Kaden, T. A. *J. Chem. Soc., Dalton Trans.* **2005**, 1136.

Scheme 2. Illustration of How the Formation of $[\text{Cu}(\text{L}2)]^{2+}$ Can Be Considered to Consist of the Initial Deprotonation of the Amino Group Followed by the Substitution of Coordinated Water



for macrocycles containing a pendant arm with a nitrogen donor, as revealed by the k_{Cu} values found for the reaction of Cu^{2+} with the $[\text{H}_3\text{L}]^{3+}$ ($\text{L} = \text{L}2, \text{L}3$) species, which are almost 4 orders of magnitude slower than those for the reaction with the related open-chain $\text{H}_3\text{tren}^{3+}$ species.⁴²

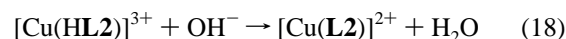
$$k = \frac{a}{1 + b[\text{H}^+]} \quad (15)$$



To complete our understanding of the kinetic properties of the Cu^{2+} complexes with these ligands, some attempts were also made to obtain information about the kinetics of the process in eq 10 and its reverse because they represent one of the most interesting functional features of these scorpionands, the movement of the tail associated to the coordination–dissociation of the pendant arm. It must be pointed out that despite the interest of these on/off reactions of the amino group in the pendant arm of macrocyclic ligands, kinetic information about these processes is almost inexistent.⁴⁷ Kinetic experiments carried out by mixing solutions of the $[\text{Cu}(\text{L}2)]^{2+}$ or $[\text{Cu}(\text{L}3)]^{2+}$ complexes with H^+ solutions with concentrations significantly lower than those used in the experiments of Figure 9 always resulted in the process being completed within the mixing time of the stopped-flow instrument, which indicates that the Cu–N bond with the amino group in the pendant arm is extremely labile. Some information about the kinetics of the reverse process, coordination of the pendant arm, could be obtained for the case of the **L2** complex. The species distribution curves for solutions containing Cu^{2+} and **L2** at a 1:1 molar ratio indicate that complex formation is only partial but significant at $\text{pH} = 3$, $[\text{Cu}(\text{HL}2)]^{3+}$ being the major complex formed under these conditions. In agreement with the results obtained in the kinetic studies on complex formation and decomposition, the spectra of these solutions show a band at 690 nm. Mixing these solutions in the stopped-flow instrument with MES or MOPS solutions buffered at pH values within the 6–8 range results in the rapid appearance of the band typical of $[\text{Cu}(\text{L}2)]^{2+}$, the process occurring always within the mixing time of the instrument (less than 2 ms). However, when the $[\text{Cu}(\text{HL}2)]^{3+}$ solutions are mixed with dilute NaOH solutions some measurable spectral changes could be observed. Because of the limited amount of OH^- available, conversion to $[\text{Cu}(\text{L}2)]^{2+}$ is not complete and the absorption maximum at equilibrium is midway

between those of $[\text{Cu}(\text{HL}2)]^{3+}$ and $[\text{Cu}(\text{L}2)]^{2+}$. As the OH^- concentration must be kept low to make the process slow enough to be measured, the spectral changes observed are small but they still allow the derivation of an approximate value of $k_{\text{on}} = (4 \pm 1) \times 10^3 \text{ dm}^3 \text{ mol}^{-1} \text{ s}^{-1}$ for the second-order rate constant corresponding to the reaction in eq 18. As indicated in Scheme 2, this reaction actually consists of two processes, deprotonation of the uncoordinated amino group by OH^- , which must be surely a diffusion-controlled process with equilibrium constant K_{OH} , and coordination of this group to the metal ion with a rate constant $k_{-\text{H}_2\text{O}}$, so that the value of k_{on} must be equal to the product $K_{\text{OH}} \times k_{-\text{H}_2\text{O}}$. The value of K_{OH} is considered to be close to that of the equilibrium constant for the reaction of the terminal NH_2 groups in uncomplexed tren species with OH^- , so it is estimated to be on the order of 10^3 – 10^5 M^{-1} , thus allowing an estimation of $k_{-\text{H}_2\text{O}}$, which must be close to 10^0 – 10^{-2} s^{-1} . These figures are much smaller than expected for the substitution of a molecule of water coordinated to Cu^{2+} by an entering neutral amino group, which indicates that the process is kinetically controlled by the structural reorganization of the complex, which includes the movement of the pendant arm. Interestingly, Siegfried and Kaden⁴⁷ also found that the rates of these processes in some related systems are independent of the lability of the metal ion.

Although the formation of only small amounts of $[\text{Cu}(\text{HL}3)]^{3+}$ in solution and the observation of only small spectral changes for $[\text{Cu}(\text{HL}3)]^{3+}$ hinder a more detailed kinetic study of these on/off processes, the results available clearly indicate that the movement of the arm of these scorpionands is very rapid in both directions, so pH changes lead to fast movements that can be signaled by the changes in the electronic spectra (Scheme 2). Further work is in progress in an attempt to make related systems with larger spectral changes associated with the molecular movement.



Conclusions

The chemistry of the new scorpionand-type pyridinophanes **L2** and **L3** provides evidence of molecular motions driven either by changes in pH only or by changes in pH coupled to the presence of Cu^{2+} ions. The crystal structure for the salt of the monoprotonated species $[\text{H}(\text{L}3)]\text{ClO}_4 \cdot \text{H}_2\text{O}$ shows a folded conformation of the pendant arm incorporating the naphthalene ring, which is placed above the macrocyclic core by means of a hydrogen bond formed between the secondary amino group of the macrocycle and the secondary amine group of the tail. π – π stacking between the aromatic rings contributes to the folding movement. However, in the salt

(47) Siegfried, L.; Kaden, T. A. *J. Chem. Soc., Dalton Trans.* **2005**, 3079.

of the triprotonated species $[\text{H}_3(\text{L3})](\text{H}_2\text{PO}_4)_3 \cdot \text{H}_2\text{O}$, the protonated tail disposes far from the discharged or diprotonated macrocyclic core macrocycle in order to minimize Coulombic repulsions. The dihydrogenphosphate anions present in the crystal are hydrogen bonded to the ammonium groups of the macrocycle and the tail. That the molecular folding also occurs in solution is evidenced by the analysis of the ^1H NMR, UV-vis, and fluorescence emissive properties of **L3**. The spectroscopic data in combination with the distribution diagrams derived from the protonation data indicate that the folding movements occur with the passage from the triprotonated to the diprotonated form of the ligand. The analysis of the NMR and potentiometric data indicates that **L2** has a similar behavior in solution. The crystal structures of $[\text{Cu}(\text{L2})](\text{ClO}_4)_2 \cdot 2\text{H}_2\text{O}$ and $[\text{Cu}(\text{L3})](\text{ClO}_4)_2$ show that in both cases the donor atom in the tail binds the metal ion so that the Cu^{2+} ions are five-coordinated. In the case of **L3**, similarly to that of the protonated free ligand, π - π stacking between the pyridine and naphthalene rings is observed. Kinetic studies on the decomposition and formation of the Cu^{2+} complexes provide additional information about the pH-dependent molecular reorganizations. Moreover, although the possibility of pH-jump stopped-flow experiments is severely limited in the present case by the species distributions and the time scale of the movement, some information was obtained to suggest that the kinetics of the tail on/off processes is essentially independent of the lability of the metal center.

Further studies are currently carried out to prepare and study systems in which the pH-driven and pM-driven metal movements can be better signaled through changes in their spectroscopic characteristics.

Experimental Section

5-Tolylsulphonylaminoethyl-2,8-ditolylsulphonyl-2,5,8-triaza[9]-2,6-pyridinophane (L2·3Ts). 2,6-Bis(bromomethyl)pyridine (1.51 g, 5.70 mmol) in dry CH_3CN (100 mL) was slowly added dropwise over a mixture of tris[2-(*N*-tolylsulphonylaminoethyl)]amine¹⁸ (3.50 g, 5.70 mmol) and K_2CO_3 (7.90 g, 57 mmol) in refluxing CH_3CN (400 mL) under argon for 20 h. Then the solution was filtered, and the solid was washed thoroughly with more CH_3CN . The combined organic layers were concentrated in a vacuum to give a white solid that was recrystallized from EtOH (1.73 g, 43%).

^1H NMR (CDCl_3 , 300 MHz): δ_{H} 7.75–7.68 (m, 7H), 7.36–7.28 (m, 8H), 5.05 (t, $J = 6$ Hz, 1H), 4.31 (s, 4H), 3.06 (t, $J = 7$ Hz, 4H), 2.87–2.81 (m, 2H), 2.45 (s, 6H), 2.41 (s, 3H), 2.36 (t, $J = 7$ Hz, 2H), 2.31 (t, $J = 7$ Hz, 4H). ^{13}C NMR (CDCl_3 , 75.43 MHz): δ_{C} 155.5, 144.1, 143.9, 139.2, 137.1, 136.1, 130.2, 127.4, 124.1, 55.1, 54.2, 52.2, 45.9, 40.9, 21.9.

5-(2-Aminoethyl)-2,5,8-triaza[9]-2,6-pyridinophane Tetrabromohydrate (L2). **L2·3Ts** (3.84 g, 5.40 mmol) and phenol (19.38 g, 206 mmol) were dissolved in 210 mL of 33% HBr/HAc, and the mixture was heated at 90 °C with stirring for 24 h. The solid obtained was filtered off and washed with a mixture of EtOH/ CH_2Cl_2 (1:1). The macrocycle was obtained as its hydrobromide salt (2.64 g, 85%).

^1H NMR (D_2O , 300 MHz): δ_{H} 7.95 (t, $J = 8$ Hz, 1H), 7.44 (d, $J = 8$ Hz, 2H), 4.63 (s, 4H), 3.29–3.21 (m, 6H), 3.02 (t, $J = 7$ Hz, 2H), 2.92 (t, $J = 5$ Hz, 4H). ^{13}C NMR (D_2O , 75.43 MHz): δ_{C}

149.2, 140.1, 122.5, 52.3, 50.9, 49.8, 46.2, 35.6, 30.5. Anal. Calcd for $\text{C}_{13}\text{H}_{23}\text{N}_5 \cdot 4\text{HBr}$: C, 27.25; H, 4.74; N, 12.22. Found: C, 27.94; H, 5.11; N, 11.86.

5-[2-(*N*-1-Naphthyl)ethylamino]-2,5,8-triaza[9]-2,6-pyridinophane Trichlorohydrate (L3). **L2** (1.43 g, 5.73 mmol) and naphthalene-1-carbaldehyde (0.90 g, 5.73 mmol) were stirred for 2 h in 150 mL of dry ethanol. NaBH_4 (0.22 g, 57 mmol) was then added and the resulting solution stirred for 1 h at room temperature. The ethanol was removed at reduced pressure. The resulting residue was treated with water and dichloromethane. The organic phase was removed at reduced pressure, and the resulting residue was dissolved in ethanol and precipitated as a hydrochloride salt (**L3**).

^1H NMR (D_2O , 300 MHz): δ_{H} 8.14 (d, $J = 8$ Hz, 1H), 8.07 (t, $J = 7$ Hz, 2H), 7.96 (t, $J = 8$ Hz, 1H), 7.58–7.75 (m, 4H), 7.45 (d, $J = 8$ Hz, 2H), 4.82 (s, 2H), 4.62 (s, 4H), 3.43 (t, $J = 8$ Hz, 2H), 3.25 (t, $J = 6$ Hz, 4H), 3.09 (t, $J = 7$ Hz, 2H), 2.91 (t, $J = 5$ Hz, 4H). ^{13}C NMR (D_2O , 75.43 MHz): δ_{C} 140.1, 132.3, 131.0, 129.9, 129.5, 127.8, 127.1, 125.9, 122.8, 122.5, 51.2, 50.8, 49.7, 48.8, 46.2, 43.1. Anal. Calcd for $\text{C}_{24}\text{H}_{31}\text{N}_5 \cdot 3\text{HCl} \cdot 1.5\text{H}_2\text{O}$: C, 54.81; H, 7.09; N, 13.31. Found: C, 55.10; H, 7.42; N, 13.38.

EMF Measurements. The potentiometric titrations were carried out at 298.1 ± 0.1 K using 0.15 M NaClO_4 as supporting electrolyte. The experimental procedure (burette, potentiometer, cell, stirrer, microcomputer, etc.) has been fully described elsewhere.⁴⁸ The acquisition of the emf data was performed with the computer program *PASAT*.⁴⁹ The reference electrode was a Ag/AgCl electrode in saturated KCl solution. The glass electrode was calibrated as a hydrogen-ion concentration probe by the titration of previously standardized amounts of HCl with CO_2 -free NaOH solutions and the equivalent point determined by the Gran's method,⁵⁰ which gives the standard potential E° and the ionic product of water ($\text{p}K_{\text{w}} = 13.73(1)$).

The computer program *HYPERQUAD* was used to calculate the protonation and stability constants.⁵¹ The pH range investigated was 2.5–11.0, and the concentration of the metal ions and of the ligands ranged from 1×10^{-3} to 5×10^{-3} mol·dm⁻³ with M/L molar ratios varying from 2:1 to 1:2. The different titration curves for each system (at least two) were treated either as a single set or as separated curves without significant variations in the values of the stability constants. Finally, the sets of data were merged together and treated simultaneously to give the final stability constants.

NMR Measurements. The ^1H and ^{13}C NMR spectra were recorded on a Bruker Avance AC-300 spectrometer operating at 299.95 MHz for ^1H and at 75.43 MHz for ^{13}C . For the ^{13}C NMR spectra, dioxane was used as a reference standard ($\delta = 67.4$ ppm), and for the ^1H spectra, the solvent signal was used as a reference standard.

Adjustments to the desired pH were made using drops of DCl or NaOD solutions. The pD was calculated from the measured pH values using the correlation, $\text{pH} = \text{pD} - 0.4$.⁵²

Spectrophotometric and Spectrofluorimetric Titrations. Absorption spectra were recorded on a Shimadzu UV-2501PC spectrophotometer. HCl and NaOH were used to adjust the pH values that were measured with a Metrohm 713 pH meter.

(48) García-España, E.; Ballester, M.-J.; Lloret, F.; Moratal, J. M.; Faus, J.; Bianchi, A. *J. Chem. Soc., Dalton Trans.* **1988**, 101.

(49) Fontanelli, M.; Micheloni, M. In *Proceedings of the I Spanish-Italian Congress on Thermodynamics of Metal Complexes*, Peñíscola, Castellón, Spain, 1990. Program for the automatic control of the microburette and the acquisition of the electromotive force readings.

(50) (a) Gran, G. *Analyst (Cambridge, U.K.)* **1952**, *77*, 661. (b) Rossotti, F. J.; Rossotti, H. *J. Chem. Educ.* **1965**, *42*, 375.

(51) Gans, P.; Sabatini, A.; Vacca, A. *Talanta* **1996**, *43*, 1739.

(52) Covington, A. K.; Paabo, M.; Robinson, R. A.; Bates, R. G. *Anal. Chem.* **1968**, *40*, 700.

Table 5. Crystallographic Data for 1–4

	1	2	3	4
empirical formula	C ₂₄ H ₃₄ N ₅ O ₅ Cl	C ₂₄ H ₄₂ N ₅ O ₁₃ P ₃	C ₂₆ H ₄₈ N ₁₀ O ₁₇ Cl ₄ Cu ₂	C ₂₄ H ₃₁ N ₅ O ₈ Cl ₂ Cu
fw	508.01	701.54	1041.62	651.98
cryst size, mm	0.15 × 0.05 × 0.1	0.05 × 0.1 × 0.1	0.05 × 0.05 × 0.1	0.05 × 0.05 × 0.1
cryst syst/space group	orthorhombic, <i>P</i> ₂₁₂₁₂₁	triclinic, <i>P</i> $\bar{1}$	monoclinic, <i>P</i> _{121/c}	monoclinic, <i>P</i> _{121/c}
<i>T</i> , K	293(2)	293(2)	293(2)	293(2)
<i>a</i> , Å	8.9370(13)	8.9080(2)	12.4470(50)	17.4360(5)
<i>b</i> , Å	16.1640(8)	12.6100(4)	19.1520(50)	10.4890(8)
<i>c</i> , Å	18.0570(19)	14.2710(5)	20.3900(50)	15.9720(10)
α , deg	90	94.530(1)	90	90
β , deg	90	100.772(1)	124.42(5)	105.551(2)
γ , deg	90	98.109(2)	90	90
<i>V</i> , Å ³	2608.5(5)	1549.89(7)	4010(2)	2814.1(3)
<i>Z</i>	4	2	4	4
<i>d</i> _{calc.} , g/cm ³	1.29	1.503	1.73	1.54
μ , mm ⁻¹	0.189	0.265	1.412	1.022
reflns collected	3434	4408	6824	3526
unique reflns	2149	2603	3426	2441
restraints	0	0	0	0
params	319	440	564	300
R1, wR2 (all)	0.065, 0.166	0.085, 0.226	0.072, 0.1764	0.1097, 0.2967
GOF	1.115	1.553	1.239	2.116

Fluorescence spectra were obtained with a PTI MO-5020 spectrofluorimeter. The emission spectra were measured from 300 to 500 nm for an excitation wavelength of 280 nm, corresponding to the maximum of the excitation intensity. HCl and NaOH were used to adjust the pH values that were measured with a Metrohm 713 pH meter.

Kinetic Experiments. The kinetic measurements were carried out with either a Cary 50-Bio spectrophotometer or an Applied Photophysics SX17MV stopped-flow instrument provided with a PDA-1 diode array detector. In both cases, the kinetic experiments provided spectral changes with time that were analyzed with the *SPECFIT* program.⁵³ All solutions for the kinetic work on complex decomposition contained Cu²⁺ and the corresponding ligand in a 1:1 molar ratio, the pH being adjusted with NaOH to values at which the formation of the CuL²⁺ complexes is complete. The kinetic experiments were carried out at 298.1 K in the presence of 0.15 dm³ mol⁻¹ NaClO₄ supporting electrolyte, the concentration of the complexes being within the range of (0.5–1.0) × 10⁻³ dm³ mol⁻¹. A similar procedure was used for the study of the on/off processes, except that the solution of acid was replaced by solutions of MES, MOPS, or NaOH. For kinetic studies on complex formation, a solution of the ligand (1–2 × 10⁻³ M) whose pH had been previously adjusted with HClO₄ and NaOH was mixed in the stopped-flow instrument with a solution of the same pH and containing the same concentration of Cu²⁺, the experiments being also carried out at 298.1 K in the presence of 0.15 dm³ mol⁻¹ NaClO₄.

Crystallographic Analysis. [H(L3)](ClO₄)·H₂O (1). Colorless crystals of (1) suitable for X-ray diffraction analysis were obtained by slow evaporation in an open vessel of aqueous solutions containing NaClO₄ 0.15 mol·dm⁻³ and L3·3HCl (0.015 g, 0.03 mmol) with an initial pH of 9. Anal. Calcd for C₂₄H₃₄N₅O₅Cl: C, 56.74; H, 6.74; N, 13.78. Found: C, 56.53; H, 7.02; N, 13.68.

Caution: Perchlorate salts of compounds containing organic ligands are potentially explosive and should be handled with care.

[H₃(L3)](H₂PO₄)₃·H₂O (2). L3·3HCl (0.021 g, 0.04 mmol) and K₂HPO₄ were mixed in 5 mL of water. The pH of the solution was adjusted to 4 by the addition of 0.1 M HCl. After the mixture was stirred for 2 h at room temperature, it was filtered and colorless crystals were obtained in 3 days by slow evaporation of the solvent in 50% yield. Anal. Calcd for C₂₄H₄₂N₅O₁₃P₃: C, 41.09; H, 6.03; N, 9.98. Found: C, 41.17; H, 6.31; N, 10.02.

[[Cu(L2)](ClO₄)₂·H₂O (3). To an aqueous solution (5 mL) of L2·4HBr (0.017 g, 0.03 mmol), Cu(ClO₄)₂·6H₂O (0.011 g, 0.03 mmol) in water (5 mL) was added dropwise with stirring. The pH of the solution was adjusted to 7 by the addition of 0.5 M NaOH. After the mixture was stirred for 2 h at room temperature, it was filtered. Blue crystals were obtained in 50% yield by slow evaporation of the solvent. Anal. Calcd for C₂₆H₄₈N₁₀O₁₇Cl₄Cu₂: C, 29.98; H, 4.64; N, 13.45. Found: C, 30.05; H, 4.71; N, 13.35.

[Cu(L3)](ClO₄)₂ (4). To an aqueous solution (5 mL) of L3·3HCl (0.017 g, 0.03 mmol), Cu(ClO₄)₂·6H₂O (0.011 g, 0.03 mmol) in water (5 mL) was added dropwise with stirring. The pH of the solution was adjusted to 7 by the addition of 0.5 M NaOH. After the mixture was stirred for 2 h at room temperature, it was filtered. Blue crystals were obtained in 50% yield by the slow evaporation of the solvent in 50% yield. Anal. Calcd for C₂₄H₃₁N₅O₈Cl₂Cu: C, 44.21; H, 4.79; N, 10.74. Found: C, 44.30; H, 4.83; N, 10.80.

Analyses on single crystals of the ligands were carried out with an Enraf-Nonius KAPPA CCD single-crystal diffractometer ($\lambda = 0.71073$ Å). The structure was solved by the Patterson method using the program *SHELXS-86*,⁵⁴ running on a Pentium 100 computer. Isotropic least-squares refinement was performed by means of the program *SHELXL-93*.⁵⁵ Some of the hydrogen atoms were located in the electron-density map, and the rest of them were geometrically fixed. Crystal data, data collection parameters, and results of the analyses are listed in Table 5. In the case of 3, the hydrogen atoms of the OH groups of dihydrogenphosphate were not located in the Fourier maps. The high *R* value in the fitting of 4 can be ascribed to the presence of a disordered perchlorate anion.

During the final stages of the refinement, the positional parameters and the anisotropic thermal parameters of the non-hydrogen atoms were refined. The hydrogen atoms were refined with a common thermal parameter. Molecular plots were produced with the program *ORTEP*.⁵⁶

(53) Binstead, R. A.; Jung, B.; Zuberbühler, A. D. *SPECFIT-32*; Spectrum Software Associates: Chapel Hill, NC, 2000.

(54) Sheldrick, G. M.; Kruger, C.; Goddard, R. *Crystallographic Computing*; Clarendon Press: Oxford, England, 1985; p. 175.

(55) Sheldrick, G. M. *SHELXL-93: Program for Crystal Structure Refinement*; Institut für Anorganische Chemie, University of Göttingen: Göttingen, Germany, 1993.

(56) Johnson, C. K. *ORTEP*; Report ORNL-3794, Oak Ridge National Laboratory: Oak Ridge, TN, 1971.

Acknowledgment. Financial support from DGICYT project CTQ2006-15672-CO5-01 and CTQ2006-14909-CO2-01 (Spain) is gratefully acknowledged. A.F. acknowledges a grant from the “Programa de Doctorado Conjunto entre la Universidad de Cádiz y las Universidades Cubanas” program (Spain). S.B. thanks MCYT of Spain for a predoctoral fellowship.

Supporting Information Available: Figure S1, Interconnections between $[H(L3)]^+$ cations, perchlorate anions and water molecules in the crystal lattice of (**1**); Figure S2, pH dependence of the absorption spectra of **L3**; Figure S3, pH dependence of the

fluorescence emission spectra of **L3**; Figure S4, ^{13}C NMR spectra in D_2O of **L2** recorded at (A) pD = 3.3, (B) pD = 8.5, (C) pD = 9.3, (D) pD = 12.6; Figure S5, 1H NMR spectra in D_2O of **L2** recorded at (A) pD = 3.3, (B) pD = 8.5, (C) pD = 9.3; Table S1, 1H chemical shifts in D_2O of **L3** recorded at (A) pD = 1.6, (B) pD = 4.1, (C) pD = 8.2, (D) pD = 9.4; Table S2, 1H and ^{13}C NMR chemical shifts in D_2O of **L2** recorded at (A) pD = 3.3, (B) pD = 8.5, (C) pD = 9.3, (D) pD = 12.6. This material is available free of charge via the Internet at <http://pubs.acs.org>.

IC700643N